Dusty Plasmoids Ejected from Silicon by Localized Microwaves - Reflection Analysis

Y. Meir and E. Jerby*
Faculty of Engineering, Tel Aviv University, Ramat Aviv, Israel.
* E-mail: jerby@eng.tau.ac.il

This paper presents an experimental and theoretical investigation of plasmoids, in forms of fireballs and fire-columns, obtained by directing localized microwaves (~0.8 kW at 2.45 GHz) into a solid substrate (e.g. silicon) in a microwave cavity. The plasmoid is blown up from the hotspot created in the silicon substrate to the air atmosphere within the microwave cavity. The experimental diagnostics utilize the microwave reflections from the dusty plasmoid in order to estimate its effective permittivity. Taking into account also prior measurements by optical spectroscopy and small-angle X-ray scattering, the electron density is estimated as $n_e \sim 3\cdot10^{18}$ m^{-3} *within the fireball.*

Keywords: Ball lightning, plasmoids, microwave plasma, atmospheric plasma, silicon spheres.

INTRODUCTION

The ejection of fireballs by localized microwaves from solid substrates and their buoyancy in air [1] has been demonstrated for various substrate materials, e.g. glass, germanium, silicon, salty water, and also for copper (forming of a fire-column-like plasma) [2]. Borosilicate-glass fireballs have also been investigated by small-angle X-ray scattering (SAXS), which revealed the presence of nanoparticles with diameters and number densities of ~50 nm and ~10^{15} m^{-3}, respectively, within these fireballs [3,4]. In view of the significant presence of dust grains compared to electrons and ions, these fireballs are considered as complex (dusty) plasmas, such as in [5]. In the present study, we analyze the microwaves reflected from the plasmoid in order to characterize its properties. Accompanied with an optical spectral analysis, which reveals the plasmoid's temperature, the microwave reflection analysis provides a measure for the plasmoid's complex permittivity and consequently for its electron density.

MATERIALS AND METHODS

The plasmoid investigated in this study is obtained by directing localized microwave power by a moveable electrode into a vertically positioned slice of silicon. A hotspot is created, from which the plasma is ejected and lifted up into the air atmosphere as a buoyant fireball within the microwave cavity [1]. The experimental setup depicted in Fig. 1a consists of a microwave cavity made of a WR340 waveguide with additional openings (in microwave cutoff) for diagnostics. These include video imaging and optical spectroscopy (Avantes, Avaspec-3648) in a 200-1000 nm range with 0.3 nm resolution. The microwave power is generated by a 2.45-GHz, 1-kW magnetron unit, fed by a controllable switched-mode power supply (MagDrive-1000, Dipolar Ltd.). The microwave is delivered to the chamber via an isolator and an impedance auto-tuner (Homer, S-Team Ltd.). The auto-tuner enables adaptive impedance matching and optimal transmission of microwave power to the fireball chamber, and it also provides real-time measurements of the complex load impedance.

The hotspot evolves at the contact point between the movable electrode and the substrate (see Fig. 1a) by a thermal-runaway process [6]. This localized-heating effect leads to melting of the substrate in a ~1 mm region near the electrode. Further heating of the hotspot results in evaporation and ionization of the substrate material. A fire column is ejected from the hotspot, and evolves as a buoyant luminous body floating stably in the air in a self-organized manner [1] as shown in Fig. 1b.

RESULTS AND DISCUSSION

A significant increase in the microwave power absorption at 2.45 GHz was observed after the fireball ignition. This effect is displayed by the reduction of the reflection coefficient $\Gamma = \rho\exp(j\theta)$ in the scalar and vectorial representations in Figs. 2a-d. The scalar microwave reflection shown in Fig. 2a is significantly decreased (from ~0.9 to ~0.5) at the fire-column ignition. The reflection is decreased

further at the fireball stage, while bouncing around ~0.3 and attracted by the Smith-chart origin as shown in Figs. 2b-d. The corresponding power reflection is reduced further to ~10% at this stage, hence the plasmoid tends to interact with its microwave generator as a nearly perfect load. These results reveal the adaptive impedance-matching effect, which dictates the plasmoid's autonomous evolution. The fluctuations observed in the fireball stage in Fig. 2d are attracted by the origin of the Smith chart (at which $\rho = 0$) in an oscillatory manner. This self-tuning mechanism tends to adaptively maximize the microwave power absorbed by the fireball, by an optimization of its intensity, position and size.

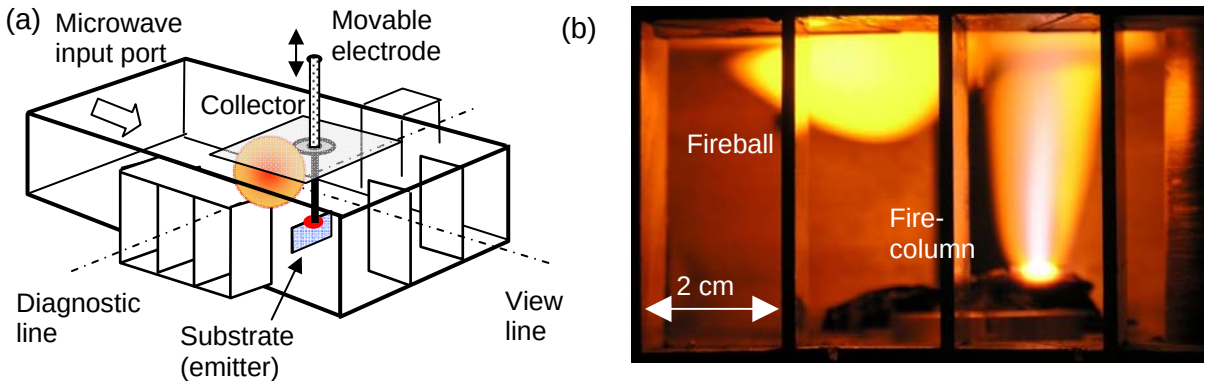

Figure 1. (a) The experimental setup. (b) A fire-column ejected from a hotspot, feeding an adjacent fireball.

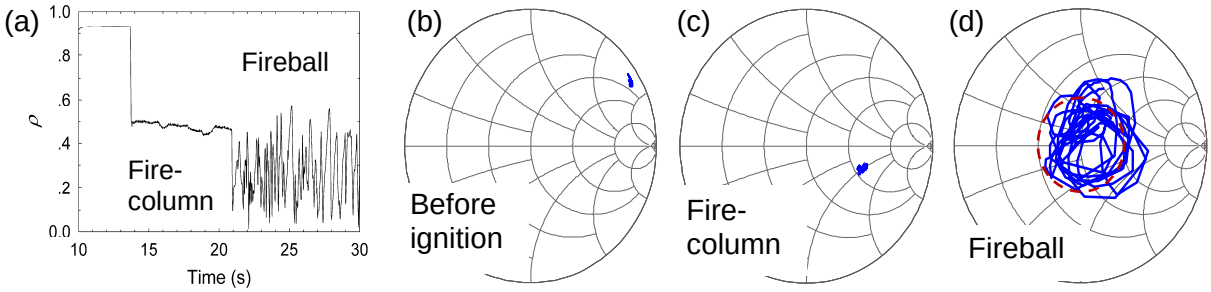

Figure 2. (a) The scalar microwave reflections before and after ignition. Smith-chart presentations of the cavity's input impedance, (b) before ignition, (c) during the fire-column, and (d) in the consequent fireball stage (the dashed circle in Red marks the $\rho = 0.33$ locus).

Silicon lines are identified in the optical spectrum [7] as well as chromium impurities. In addition, spectral emissions of nitric oxide (NO) and hydroxyl (OH^-) radicals are observed. When using a graphite electrode, cyano (CN) radicals are also generated within the plasmoid. The radicals' spectra are used to estimate the rotational temperature by fitting the line shape to the LifBase simulation [8]. The OH^- and CN radicals result in mean temperatures of 0.34 ± 0.04 eV and 0.40 ± 0.11 eV, respectively. The Boltzmann plot method applied on silicon lines reveals an excitation temperature of ~1 eV. Chromium impurities, probably originating from the electrode, yield an excitation temperature of ~0.3 eV in a similar manner (the better accuracy in this instance compared to that obtained with silicon is attributed to the larger number of chromium spectral lines, the partial overlap of the silicon lines and NO radical emission, and the relatively low spectral resolution and sampling available). From SAXS measurements [3, 4], the mean particle radius r is ~60 nm, their number density n_d is ~10^{15}-10^{16} m^{-3}, and their maximum volume fraction is ~10^{-6} within the fireball.

The measured microwave reflections enable us to estimate the effective plasmoid impedance, and consequently to find its relative dielectric permittivity, ε_r . The latter consists of the plasma permittivity $\varepsilon_p = \varepsilon_p' - j\varepsilon_p''$ and the dust conductivity, σ_{ed} , thus the total effective permittivity is given by $\varepsilon_r = \varepsilon_p - j\sigma_{ed}/\varepsilon_0\omega$ where ε_0 is the vacuum permittivity and ω is the angular frequency.

The dielectric permittivity of the dusty plasma is determined by $\omega_p = \sqrt{e^2 n_e / m_e \varepsilon_0}$ and υ, the plasma and collision frequencies, respectively. Therefore, the dusty plasma conductivity given by [5] is

$$\sigma_{ed} \cong \frac{n_e n_d \pi r^2 e^2}{m_e} \frac{\omega}{k} \left[\frac{\omega^2 - \upsilon \upsilon_{ch}}{(\omega^2 + \upsilon_{ch}^2)(\omega^2 + \upsilon^2)} + j\omega \frac{\upsilon + \upsilon_{ch}}{(\omega^2 + \upsilon_{ch}^2)(\omega^2 + \upsilon^2)} \right], \quad (1)$$

where n_e and n_d are the electron and dust grain densities, respectively, e and m_e are the electron charge and mass, respectively, and k is the wave wavenumber. The electron effective collision frequency is $\upsilon = V_{Te} \sigma_n N_n$, where $V_{Te}=(kT_e/m_e)^{1/2}$ is the electron thermal velocity, σ_n and N_n are the neutrals cross-section and density, respectively, T_e is the electron temperature, and υ_{ch} is the dust charging frequency. Assuming $\upsilon \upsilon_{ch} \ll \omega^2$ and $\upsilon_{ch} \ll \omega$ in (1), the dielectric permittivity is further reduced to

$$\varepsilon_r \simeq 1 + \frac{\omega_p^2}{\omega^2 + \upsilon^2} \left[-1 + \frac{\upsilon}{k l_d \omega} - j \left(\frac{\upsilon}{\omega} + \frac{1}{k l_d} \right) \right] g, \quad (2)$$

where $l_d = 1/\pi r^2 n_d$ is defined here as the mean free path for electron-dust collisions, and g is a spatial profile distribution function. The model illustrated in Fig. 3a is employed using COMSOL MultiPhysics™ in order to estimate the corresponding permittivity of the plasmoid, ε_r, from the reflection coefficient measurements, Γ, as in Fig. 2d. A Gaussian profile g is taken for the plasmoid with a 1-cm and 1.6 cm radii of its core in the radial and axial dimensions, respectively. A ~1 mm sheath barrier is assumed between the plasmoid and the waveguide ceiling. The complex ε_r space is scanned numerically in order to find the conditions that satisfy $\rho \le 0.33$ as experimentally observed.

The amplitude profile of the displacement field $\mathbf{D} = \varepsilon_0 \varepsilon_r \mathbf{E}$ along the waveguide is presented in Fig. 3a for $\varepsilon_r = 0.2 - j20$ (in which the reflections attain $\rho \le 0.33$). The corresponding reflection coefficients are shown in Fig. 3b as functions of the axial position (i.e. as indicated in Fig. 3a) for several values of ε_r. A nearly perfect impedance matching (no reflection) is observed for $\varepsilon_r = 0.2 - j20$ at 35 mm axial position. Other positions or higher dielectric losses of the plasmoid decrease its microwave absorption. This effect is illustrated also by the Smith-chart presentation in Fig. 3b, which maps the complex relation between ε_r and the microwave reflection coefficient Γ, in various positions. The area within the dashed Red circle marks the $\rho \le 0.33$ region, with less than 10% microwave power reflection. A longitudinal periodicity of about half a wavelength is notable.

The electron temperatures in the range of 0.3–1.0 eV, yield an electron thermal velocity of $V_{Te} \sim 2.3 \cdot 10^5$ ms^{-1} hence the collision frequency is $\upsilon \sim 10^{10}$ s^{-1} (assuming $\sigma_n \sim 4.4 \cdot 10^{-20}$ m^2 and $N_n \sim 10^{24}$ m^{-3} for a weakly ionized dusty plasma in air atmosphere [5]). The SAXS measurements yield a mean free path for electron-dust collisions of $l_d \sim 10^{-2}$ m. In these conditions, for $\omega \sim 1.6 \cdot 10^{10}$ s^{-1}, the real part in Eq. (2), $-1 + \upsilon / k l_d \omega \sim 0$, is significantly smaller than the imaginary part, which plays the dominant role in the microwave absorption by the plasmoid. Hence, the plasma frequency results in $\omega_p \sim 10^{11}$ s^{-1} with corresponding electron density of $n_e \sim 3 \cdot 10^{18}$ m^{-3} in this case.

CONCLUSIONS

The fireball studied here is categorised as a partially ionized complex (dusty) plasma, as indicated by the low electron density estimated, the low temperatures measured, the lack of atomic ionization spectral lines, and the presence of nanoparticles forming the dusty plasmoid ($n_e \sim 3 \cdot 10^{18}$ m^{-3}, $n_d \sim 10^{15}$ m^{-3}). The measured electron density is slightly lower than the limit derived by Griem's criterion [9] for local thermal equilibrium (LTE); however, it may satisfy the partial-LTE (pLTE)

condition [10]. In atmospheric-pressure plasmas, the LTE assumption may be valid in the core of the plasmoid, but not on its periphery [11]. The equilibrium may exist since the higher pressure in the core increases the collision rate between the electrons and heavy particles, hence the energy transfer becomes more effective for a given electron density.

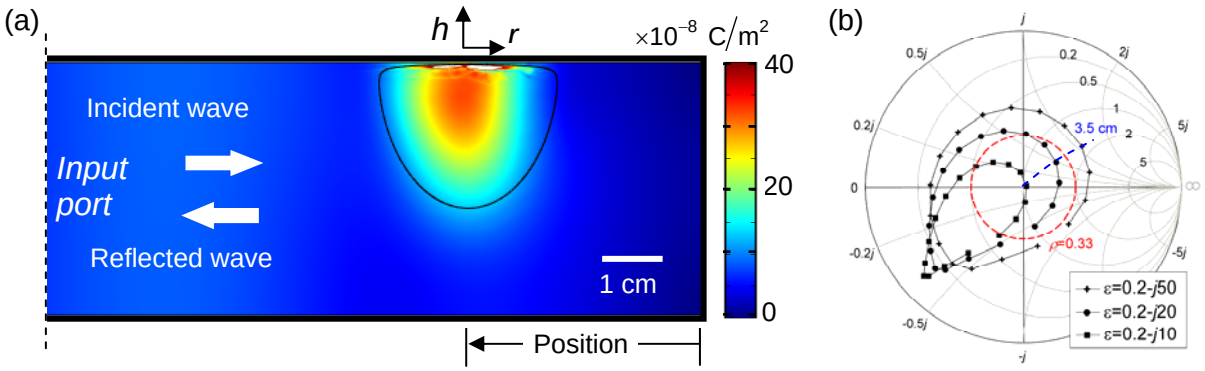

Figure 3. (a) The plasmoid shape and position used in the numerical model, and the displacement field magnitude for $\varepsilon_r = 0.2 - j20$. (b) The reflection coefficient as a function of the axial position.

The contributions of the electron and dust components to the total value of ε_r in Eq. (2) are comparable, hence the dust particles play a non-negligible role in the microwave absorption by the plasmoid. The fireball attraction to the Smith-chart origin is observed experimentally as the self-impedance-matching effect presented in Fig. 3b. This is an oscillatory effect since once the fireball is perfectly matched, more power is absorbed, which increases the electron density (e.g. along the blue curve in Fig. 3b). The consequent increase in the plasmoid conductivity violates the perfect matching condition, causing the system to bounce back and forth around its equilibrium state, as was also observed experimentally.

ACKNOWLEDGEMENTS

This study is supported by the Israel Science Foundation (ISF) under grant No. 1639/11.

REFERENCES

[1] Dikhtyar V. and Jerby E., Fireball ejection from a molten hot-spot to air by localized microwaves *Phys. Rev. Lett.* **96**, pp. 045002-1-4, 2006.

[2] Jerby E., Golts A., Shamir Y., Wonde S., Mitchell J. B. A., LeGarrec J. L., Narayanan T., Sztucki M., Ashkenazi D., Barkay Z. and Eliaz N., Nanoparticle plasma ejected directly from solid copper by localized microwaves *Appl. Phys. Lett.* **95**, pp. 191501-1-3, 2009.

[3] Mitchell J. B. A., LeGarrec J.L., Sztucki M., Narayanan T., Dikhtyar V. and Jerby E., Evidence for nanoparticles in microwave-generated fireballs observed by synchrotron X-ray scattering, *Phys. Rev. Lett.* **100** pp. 065001-1-4, 2008.

[4] Jerby E., Meir Y., Barkay Z., Ashkenazi D., Mitchell J. B., Narayanan T., Eliaz N., LeGarrec J. L., Sztucki M., Meshcheryakov O. and Balaish A., Experimental characterization of silica plasmoids excited by localized microwaves in air atmosphere *Microwave Discharges, Fundamentals and Applications, Proc. MD-8*, Sept. 10-14, 2012, pp. 141-146, Yanus-K, Moscow.

[5] Xiang S. Y., Biao G. D, and Jian W., Theoretical analysis of microwave attenuation constant of weakly ionized dusty plasma *Chin. J. Geophys.* **50**, pp. 877-883, 2007.

[6] Jerby E., Aktushev O. and Dikhtyar V. Theoretical analysis of the microwave-drill near-field localized heating effect *J. Appl. Phys.* **97**, pp. 034909-1-7, 2005.

[7] Meir Y. and Jerby E., Breakdown spectroscopy induced by localized microwaves for material identification *Microw. Opt. Technol. Lett.* **53**, pp. 2281-2283, 2011.

[8] Luque J. and Crosley D.R., *LIFBASE;* SRI Int'l Report MP 99-009, USA, 1999.

[9] Griem H. R., *Plasma spectroscopy*, New York: McGraw-Hill, 1964.

[10] Griem H. R., Validity of local thermal equilibrium in plasma spectroscopy *Phys. Rev.* **131**, pp. 1170-1176, 1963.

[11] Tendero C., Tixier C., Tristant P., Desmaison J. and Leprince P., Atmospheric pressure plasmas: A review *Spectrochim. Acta Part B At. Spectrosc.* **61**, pp. 2-30, 2006.